# Joint Centre for Mesoscale Meteorology, Reading, UK

# Verification of the Tracking Technique Used in an Experimental Cloud Motion Wind Inferring System

K. A. Browning
Z. Wang
G. A. Kelly

Internal Report No. 78

October 1997

**Met Office** Joint Centre for Mesoscale Meteorology Department of Meteorology
University of Reading PO Box 243 Reading RG6 6BB United Kingdom
Tel: +44 (0)118 931 8425 Fax: +44 (0)118 931 8791
www.metoffice.com

*Designed and produced by the Met Office © Crown copyright 2001 01/0240 The Met Office logo is a registered trademark.*

# Verification of the Tracking Technique Used in an Experimental Cloud Motion Wind Inferring System

By Z. WANG[*1], K. A. BROWNING[1] and G. A. KELLY[⇕2]

[1] University of Reading

[2] European Centre for Medium-Range Weather Forecasts

Submitted to
*Quarterly Journal of the Royal Meteorological Society*

October 1997

[*] Permanent address: Department of Atmospheric Physics, Nanjing Institute of Meteorology, Nanjing 210044, P.R.C.

[⇕] Corresponding author: European Centre for Medium-Range Weather Forecasts, Shinfield Park, Reading RG2 9AX, U.K.

# Verification of the Tracking Technique Used in an Experimental Cloud Motion Wind Inferring System

By Z. WANG[*1], K. A. BROWNING[1] and G. A. KELLY[⇕2]

[1] University of Reading

[2] European Centre for Medium-Range Weather Forecasts

## SUMMARY

An auto-adapting tracking technique, independent of the first guess to wind field, has been designed to extract cloud motion wind(CMW) vectors from geostationary satellite images. It has been implemented as a PC-based experimental cloud-motion wind-inferring system. The system uses procedures to improve the computing efficiency and increase the amount and reliability of cloud motion information. The resulting cloud motion wind vectors, each of which is marked with a quality flag(QF), are compared with model winds and direct observations obtained during the Fronts and Atlantic Storm Track Experiment(FASTEX).

The comparison of the CMW vectors with operational numerical model analyses(and 3-hour forecasts) from the United Kingdom Meteorological Office shows that the bias and rms speed difference, and the rms vector difference are -0.6, 3.2 and 6.1 $ms^{-1}$ for a particular setting of quality flag(QF>1600). Comparison with the operational numerical model 3-hour forecasts from the European Centre for Medium-Range Weather Forecasts gives slightly worse results in general but it appears that CMW fields are closer to ECMWF model at low levels and to UKMO model at high and medium levels.

The comparison with direct observations from dropsondes, radiosondes, buoys and ships, shows that, given QF>1600, the bias and rms speed difference and rms vector difference of the cloud motion wind vectors averaged over all levels are 0.4, 5.5 and 8.3 $ms^{-1}$, respectively. These values are marginally better than the numerical analyses(and 3-hour forecasts) from either the UKMO model which gives corresponding values of -0.2, 5.7 and 9.5 $ms^{-1}$, respectively, or from the ECMWF model which gives corresponding values of -0.5, 7.2 and 9.6 $ms^{-1}$, respectively.

[*] Permanent address: Department of Atmospheric Physics, Nanjing Institute of Meteorology, Nanjing 210044, P.R.C.

[⇕] Corresponding author: European Centre for Medium-Range Weather Forecasts, Shinfield Park, Reading RG2 9AX, U.K.

The low values of bias and rms speed difference and rms vector difference of the cloud motion wind vectors are good indicators that the method works well in the five cases.

KEYWORDS: Satellite images Cloud motion wind Tracking technique

## 1. INTRODUCTION

Extraction of cloud motion winds(CMW) from geostationary satellite images has been performed operationally for about 20 years and the products have been shown to be useful for weather forecasting(e.g. Schmetz et al. 1993; Marshall et al 1994; Takata 1993; Walter 1993; Kelkar et al. 1993; Kelly 1997; Tomassini et al. 1997). Many research studies on target selection, tracking algorithms, height assignment and quality control in the extraction procedure have improved the performance of wind inferring systems and the accuracy of their products.

In this paper, the auto-adapting tracking scheme used in an experimental local cloud motion wind inferring system(CWIS) is introduced. Automated editing and quality assessing of cloud motion vectors with a cross-checking scheme specifically designed for processing 4 raw CMW fields derived from 3 sequential satellite images with 2 pattern-recognition parameters are also described in detail. The technique is verified through the comparison of its outputs with the analyses from the limited-area version of the operational Unified Model of the United Kingdom Meteorological Office (Cullen 1993), referred to as the Limited Area Model(LAM), with the analyses from the medium-range weather prediction model in the European Centre for Medium-Range Weather Forecasts(Dent 1993), and with the direct observations from dropsondes, radiosondes, ships and buoys for the Fronts & Atlantic Storm Track Experiment(FASTEX) (Joly et al. 1997). Five cases were selected for study, representive of highly variable and often stormy wintertime conditions.

## 2. PATTERN RECOGNITION PARAMETER ANALYSIS

Cloud tracking in principle is based on a pattern recognition technique. After defining a target template in one image and a search area in another, an array of pattern recognition parameters is computed and analysed to find out the best matching template to the target area. The most popularly used pattern recognition parameter is the correlation coefficient(CC) between the target template T,

which has $N_t * N_t$ pixels, and a template S which has the same size as T but at a different position expressed by $(n, m)$ in the search area. CC is defined as

$$CC_{n,m} = \frac{E(TS)_{n,m} - E(T)\ E(S)_{n,m}}{\sigma_T\ \sigma_{S_{n,m}}} = \frac{E((T-\overline{T}\ )(S-\overline{S}_{n,m}))_{n,m}}{\sigma_T\ \sigma_{S_{n,m}}}$$

Where

$$E(TS)_{n,m} = \frac{1}{N_t^2}\sum_{i=1}^{N_t}\ \sum_{j=1}^{N_t}\ T_{i,j}S_{n+i,m+j}$$

$$E(T) = \overline{T}\ = \frac{1}{N_t^2}\sum_{i=1}^{N_t}\ \sum_{j=1}^{N_t}\ T_{i,j}\ ,\qquad E(S)_{n,m} = \overline{S}_{\text{n,m}} = \frac{1}{N_t^2}\sum_{i=1}^{N_t}\ \sum_{j=1}^{N_t}\ S_{n+i,m+j}$$

$$\sigma_T = \sqrt{\frac{1}{N_t^2}\sum_{i=1}^{N_t}\ \sum_{j=1}^{N_t}\ (T_{i,j}-\overline{T})^2} = \sqrt{E(TT)-E^2(T)} = \sqrt{E(T-\overline{T})^2}$$

$$\sigma_{S_{n,m}} = \sqrt{\frac{1}{N_t^2}\sum_{i=1}^{N_t}\ \sum_{j=1}^{N_t}\ (S_{n+i,m+j}-\overline{S}_{n,m})^2} = \sqrt{E(SS)_{n,m}-E^2(S)_{n,m}} = \sqrt{E(S-\overline{S}_{n,m})^2}$$

Since $E((T-\overline{T})(S-\overline{S}_{n,m}))_{n,m}$ and $\sigma_T$ and $\sigma_{S_{n,m}}$ are central moments of pixels, i.e., the means of pixel values $\overline{T}$ and $\overline{S}_{n,m}$ have been subtracted from the original pixel values in T and S, the magnitude of $CC_{n,m}$ expresses the similarity of pixels value envelopes rather than the pixel-value differences between T and S. If the two envelopes are proportional, i.e.,

$$T_{i,j} - \overline{T} \equiv k\ \ (S_{n+i,m+j} - \overline{S}_{n,m})$$

holds for a constant k at any $(i, j)$ in the template, $CC_{n,m}$ reaches its maximum of 1, leading to a perfect match.

As an alternative to $CC_{n,m}$, the minimum distance is used(e.g., Marshall et al 1994; Velden et al. 1997). The minimum distance is defined by

$$DD_{n,m} = \sum_{i=1}^{N_t}\ \sum_{j=1}^{N_t}\ (T_{i,j} - S_{n+i,m+j})^2$$

Obviously not only is it computationally faster to work out $DD_{n,m}$ than $CC_{n,m}$, but also $DD_{n,m}$ depends on the differences in pixel value and has a quite different meaning from $CC_{n,m}$. A perfect match happens when $DD_{n,m}$ =0 determined by

$$T_{i,j} \equiv\ S_{n+i,m+j}$$

for any (i,j) in the template. So for a given target template and a search area, the position of the maximum in the DD surface may be quite different from that in the CC surface. As mentioned by Buhler and Holmlund(1993), the DD surface is smoother than the CC surface, and therefore the implementation of the DD scheme at reduced resolution might provide very reliable results.

Another alternative has also been used experimentally by Wang and Zeng(1996) and is defined by

$$OC_{n,m} = \frac{E(TS)_{n,m}}{\sqrt{E(TT)\ E(SS)_{n,m}}}$$

and determined by the original moments of pixel values $E(TS)_{n,m}$, $E(TT)$ and $E(SS)_{n,m}$. So, the magnitude of $OC_{n,m}$ expresses the ratio of pixel values between T and S. If pixel values are proportional, i.e.,

$$T_{i,j} \equiv K * S_{n+i,m+j}$$

holds for a constant K at any $(i, j)$ in the template, $OC_{n,m}$ reaches its maximum of 1, leading to a perfect match in terms of $OC_{n,m}$.

The appearance of the OC surface may be different from either the CC surface or the DD surface. But in general, the OC surface, like the DD surface, is also smoother than the CC surface(Wang et al. 1991). Because of the characteristic differences in these matching surfaces, they can be used as pattern recognition parameter couples in the tracking procedure. Thus they are complementary to each other and more information can be derived from 2 or 3 match surfaces than from only one, and the signal-to-noise ratio is thereby increased. CWIS uses CC and OC as a pattern recognition parameter couple. The value of OC is experimentally transformed to its 16th power, i.e., $(OC)^{16}$, in order to be comparable with the value of CC when they are used in constructing quality flags(see Section 3b).

## 3. TRACKING TECHNIQUE

### (a) Auto-adapting algorithm for constructing correlation surfaces

Computation of a full CC surface is very time-consuming quite apart from the fact that the OC surface has to be computed at the same time. In order to save time, many algorithms use forecast wind speed and direction as a first guess to modify the size and position of the search area. The aim of CWIS is to achieve tracking that is independent of a weather forecast. An auto-adapting scheme is designed to simulate a blind person finding his way to the top of a hill. The procedure is completed in a few steps.

In the first step, a square with a width of $2r+N_t$ is used as a search area so that a correlation surface with $2r*2r$ points is constructed. If the maximum of correlation is located at the edge of the surface, the search area is moved to a new place in the direction of the maximum and a new correlation surface is computed(Fig.1). This step is repeated until a maximum of correlation is found within the surface. Of course the number of repetitions is limited according to the climatologically possible wind speed. The value of $r$ is defined by

$$r = st / p$$

where t=30 minutes and p=5km for Meteosat IR images, and s=12 $ms^{-1}$ is used in order to make a compromise between the computing efficiency and tracking effectiveness.

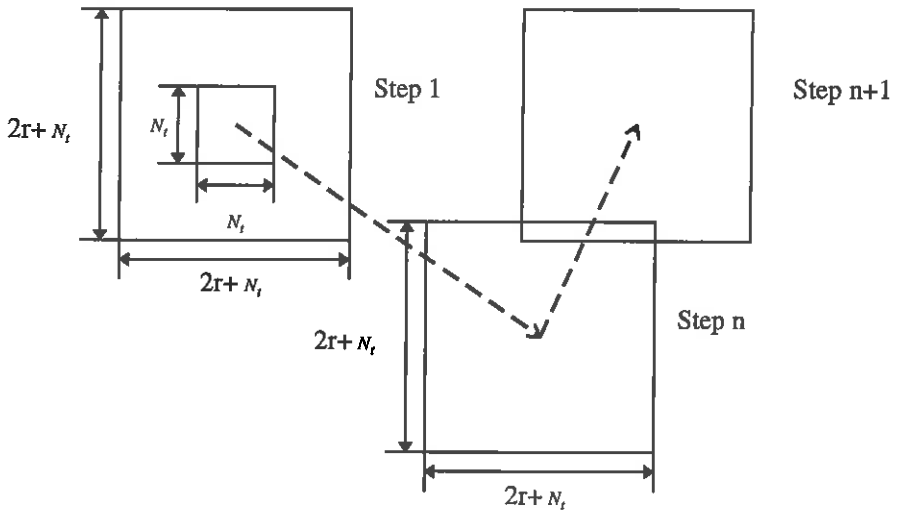


Figure 1. Schematic of auto-adapting algorithm

Using this algorithm, one may possibly lose the information given by other peaks, if they exist, in a full correlation surface. One even risks losing all the peaks in the full surface if none of these peaks is

linked with the maximum found at the first step. However, in practice only one of these peaks is taken for the determination of the final cloud motion wind(CMW) and the others are dropped as noise. And further, information lost by the CC surface may probably be retrieved by the DC surface or vice versa. The risk of losing all the peaks can be avoided by appropriately increasing the value of $r$.

(b) Automated consistency editor and quality flag

The current CWIS extracts CMW based on a triplet of IR images referred to as images A, B and C. Image B contains the target template, and A and B contain the search areas. The mean brightness temperature $\overline{T}_B$ of the coldest 15% pixels in a target template is used to interpolate an estimate of pressure height from a local (FASTEX area) mean temperature profile of a 12-hour prediction from the LAM. This $\overline{T}_B$-equivalent pressure height will be used as a parameter during CMW assimilation for height assignment(see the next subsection). The wind vectors corresponding to the displacement of the target between the image couplet BA, and between BC, are extracted. Since two pattern recognition parameters are used, CWIS provides four CMW raw fields(Fig.2) in which noise as well as wind information(signal) are included. The purpose of quality control is to extract the signal from the raw fields and leave the noise behind. Thus the final CMW field for further analysis and application is characterised qualitatively by as high as possible a signal-to-noise ratio and quantitatively by as many as possible CMW vectors. Quality control in CWIS is performed in two steps which are described in this and the next subsections.

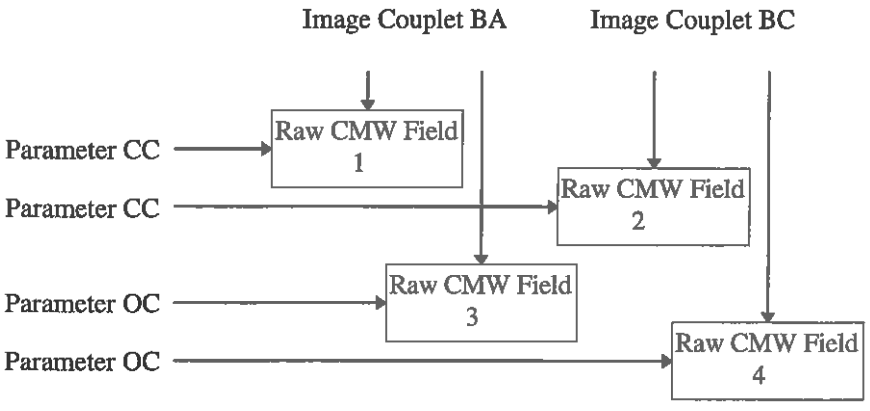


Figure 2. Schematic showing a quartet of raw CMW fields derived from a satellite imagery triplet with a pattern recognition parameter couple

The first step of quality control is the automated consistency editing. Its flow chart is given in Fig. 3. In the procedure, four raw CMW fields are cross-compared, and the spatial and temporal consistencies of CMW vectors are checked and quality flags(QF) are marked with three QC modules. Module QCA checks the CMW direction consistency with the average over its 8 neighbours. QCB checks the consistencies of CMW direction, speed and $\overline{T}_B$-equivalent pressure height. QCC compares two CMW fields to find out how different they are because of either the time difference or the pattern recognition parameter difference, and combines them into one field according to their quality and consistency. Direction consistency check for an individual CMW field is performed twice, once in QCA and another in QCB, so that direction conflicting is strictly controlled.

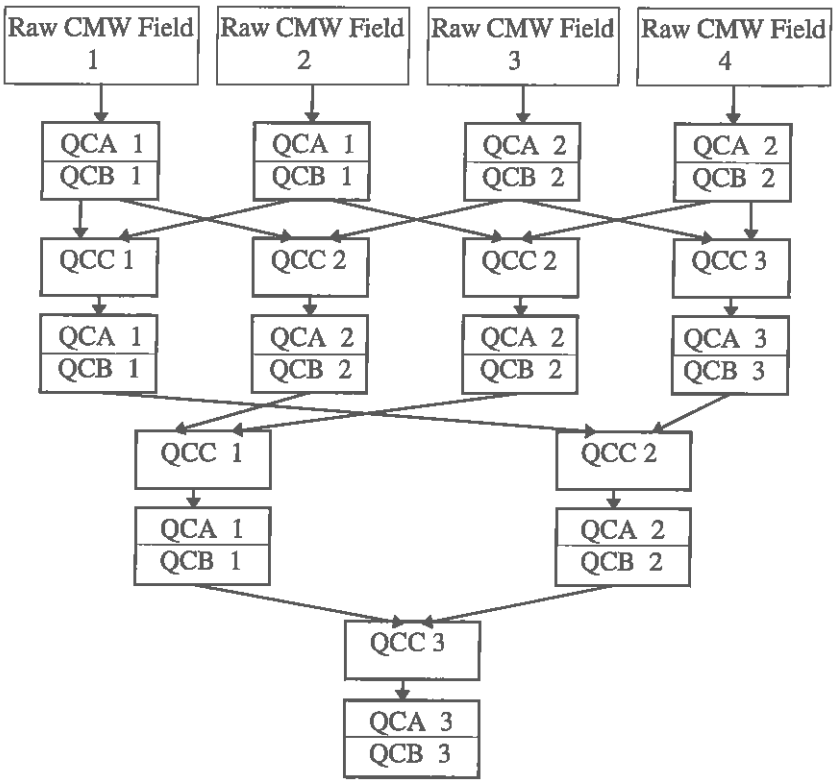


Figure 3. Flow chart for quality control

In the flow chart, the numbers following module names are criterion grades. The criteria used for consistency checking at each grade are listed in Table 1. They have been chosen experimentally based on many articles, such as Marshall et al (1994), Holmlund(1993), and Hayden(1993), and the analysis of the results generated correspondingly. In QCC, the combination is simply the average of the 2

collocated vectors, or the option of the best, or the rejection of all of them, depending on the results of consistency analysis.

TABLE 1. CRITERIA FOR WIND DIRECTION AND SPEED AND PRESSURE CONSISTENCY ANALYSIS

| Grade No. | QCA | QCB | | | QCC | |
|---|---|---|---|---|---|---|
| | $\delta d_c$ | $\delta d_c$ | $\delta s_c$ | $\delta p_c$ | $\delta d_c$ | $\delta s_c$ |
| 1 | 90 | 90 | 6.0 | 200 | 90 | 18 |
| 2 | 80 | 80 | 5.4 | 180 | 80 | 16 |
| 3 | 70 | 70 | 4.8 | 160 | 70 | 14 |

Quality flags in CMW field are initialised with 1000 multiplied by CC or OC from the maximum cross-correlation analysis, and are modified each time when a QC module is performed. The modification formula are as follows.

$$QCA: \quad QF_{new} = \begin{cases} QF_{old} + (\delta d_c - \delta d), & \delta d < \delta d_c \\ 0, & \delta d \geq \delta d_c \end{cases}$$

$$QCB: \quad QF_{new} = \begin{cases} QF_{old} + 30 * m, & m \geq 1 \\ 0, & m = 0 \end{cases}$$

$$QCC: \quad QF_{new} = \begin{cases} (QF_1 + QF_2)/2 + (\delta d_c - \delta d) + 90(1 - \delta s / \delta s_c), & in\ case 1 \\ QF_1 / 2, & in\ case 2 \\ 0, & in\ case 3 \end{cases}$$

1. $\delta d < \delta d_c$ *and* $\delta s < \delta s_c$ *(i.e., two vectors consistent),*
2. *two vectors not consistent but* $QF_1 > QF_2 > 980$ *or only one of the 2 vectors available and associated* $QF_1 > 980$,
3. *any other cases,*

where $QF_{new}$ is the value after modification, $QF_{old}$, $QF_1$ and $QF_2$ are the values before modification, and $m$ is the number of its consistent neighbouring vectors. It can be seen that, in general, QF should increase during this process. The maximum increase caused by each module is 90, 240, and 180 respectively. Since QCA and QCB are called hierarchically 4 times and QCC is called 3 times, the maximum possible value of QF at the end of consistency editing in CWIS is 2860.

(c) CMW assimilation with LAM output for height assignment

The major source of problems in the use of cloud motion wind data is due to the errors in cloud height assignment(Smith 1991). Researchers have suggested many height-assignment techniques which physically fall into 3 categories: the infrared window technique, the carbon dioxide technique, and the water vapour intercept technique(Menzel et al. 1993). Since the emphasis of this research is on the verification of the tracking algorithm described above, 12-hour forecasts made by UKMO LAM model are used to assimilate the cloud motion vectors to get better estimates of height based on the $\overline{T}_B$-equivalent pressure height given before. And for the same reason, the relationship between the $\overline{T}_B$-equivalent pressure heights and the assimilated heights is not further discussed in the following sections of this paper. Similar to the concept in Hayden(1993), a penalty function is defined as

$$F_k = [(\frac{\delta p_k}{50})^2 + (\frac{\delta d_k}{5})^2 + (\frac{\delta s_k}{1})^2]^{1/2}$$

where subscript k refers to the pressure level, $\delta p_k = p - p_k$, $\delta d_k = d - d_k$, $\delta s_k = s - s_k$ are the differences in pressure, wind speed and direction between CMW and LAM 12-hour prediction. It can be seen that the weights in the formula imply that, in terms of the contribution to the function, 1 $ms^{-1}$ difference in wind speed, 5 degree difference in wind direction and 50 hPa difference in pressure height are equivalent to each other. The pressure height, at which the function $F_k$ has a minimum, is taken as a better estimate of CMW height.

The constraint to the magnitude of this minimum, $F_{\min}$, is realised through the final modification to the value of the quality flag:

$$QF_{new} = QF_{old} + K_1(K_2 - F_{\min})$$

where $K_1$=100 and $K_2$=6. This implies that QF would be increased if $F_{\min}$<6, and would be decreased if $F_{\min}$>6. The maximum increase is 600 when $F_{\min}$=0. The final value of QF would be less than 1100 if $F_{\min}$>23.6. Thus, it is not easy to reject a CMW vector from dissemination in this step if the value of $QF_{old}$ has been quite large(Holmlund 1996).

With this assimilation scheme, for a criterion QF>1600 which will be discussed further in the next section, the linear correlation coefficient between the $\overline{T}_B$-equivalent pressure heights and the assimilated pressure heights is 0.75. The correlation varies in the same way as QF-criterion does.

The function

$$f_k = [(\frac{\delta d_k}{5})^2 + (\frac{\delta s_k}{1})^2]^{1/2}$$

is used to determine the level-of-best fit(LBF). This function is similar to the penalty function $F_k$, but the pressure term is removed and the LAM observational analysis is used in working out LBF.

## 4. RESULTS

Meteosat half-hourly IR images, LAM analyses and forecasts, ECMWF 3-hour forecasts(ECM) ,and direct observations made by dropsondes, radiosondes, ships and buoys during FASTEX Intensive Observing Periods(IOP) 11, 15, 16, 17, and 19 have been used as five cases for this research. The reference time for each of the 5 cases is Feb. 5th at 0000UTC, 15th at 0900UTC, 17th at 0900UTC, 19th at 0900UTC and 27th at 0900UTC.

Satellite images remapped onto a latitude-longitude grid (43 ° N-63 ° N, 0 ° W-50 ° W) are used as the input for CWIS. The target template size is $16 \times 16$ pixels and pixel resolution is about $5 \times 5 km^2$. A 12 or 15 -hour forecast from the LAM in the same area with output at 100hPa intervals is used to provide a mean temperature profile and complete height assignment to CMW. A 0-hour analysis from the LAM is used to assess the CMW vectors, but, if CMW vectors are derived from satellite images observed around 0900UTC, a 3-hour forecast from the 0600UTC run of the LAM is used instead. The distances between 'collocated' CMW and LAM vectors are less than 0.25 ° latitude and 0.5 ° longitude( thus, multiple collocations can exist).

Direct observations were made by dropsondes released from the UK C 130 and US Gulfstream-IV aircraft, and radiosondes launched from 19 ground-based upper-air sounding stations and 8

observing ships. Sea surface wind observations from buoys and ships are also collected for either quantitative comparison or qualitative assessment. The data were obtained from the FASTEX Archive Centre established by Meteo-France in Toulouse, France. In this study, however the UK C 130 data received from the Global Telecommunication System(GTS) code in the Archive Centre are replaced with the high-resolution data presently being derived in the Joint Centre for Mesoscale Meteorology.

(a) Qualitative assessment

Of the 5 cases, the case at 0900UTC, 15 Feb.1997(our Case 2) is given in Figure 4 as an example. This figure shows the satellite image, with the CMW field superimposed(Fig.4a), collocated LAM vectors(Fig.4b) and ECM vectors(Fig.4c) at the same height as the corresponding CMW, and directly-observed winds(Fig.4d) at the height closest to the CMW height. According to sea level pressure analysis, a low centre associated with a mature cyclone is centred at around 52 $^{\circ}$ N, 28 $^{\circ}$ W. The broad flow pattern associated with the low is well reflected by the CMW vectors in Fig.4a extracted from its associated cloud. The lack of winds over the northeast quadrant of the cyclone is due to a large area of deep layer cloud with convective tops penetrating it, which is not suitable for tracking because the life of the fine structure within the cloud patterns is not long enougth to derive consistency vectors. Around 52 $^{\circ}$ N, 40 $^{\circ}$ W, to the west of the cyclone, CMW vectors are not available because the cloud in this area is too uniform to be traceable. Winds are also lacking in the dry slot around 47 $^{\circ}$ N, 25 $^{\circ}$ W, where no cloud can be seen. Another clear region is around 50 $^{\circ}$ N, 5 $^{\circ}$ W. The quantitative comparison of CMW vectors with LAM, ECM, and direct observations will be described in Sections 4c, 4d and 4e. In this section we shall merely present the qualitative features. A visual comparison of the CMW vectors in Fig.4a with the collocated LAM 3-hour forecast winds in Fig.4b shows that they are in good agreement in general although there are a few disagreements. For example, according to Figs. 4a and 4b, the ridge-low-ridge pattern is reproduced consistently, but CMW shows the axis of the ridge on the west-side to be farther east than in the LAM, though more nearly in agreement with that in the ECM(Fig.4c). In the area around 47 $^{\circ}$ N, 40 $^{\circ}$ W, the CMW flow is generally backed by 20 $^{\circ}$ compared to the LAM but is consistent with direct observations(see Fig.4d). Two seemingly out-

of-place south-wind vectors in the CMW field at 62° N, 36° W can be eliminated by increasing the criterion of quality flag QF up to 1600. Choice of QF criterion will be discussed in the following.

Figure 4. An example of Meteosat IR image, CMW vectors and their collocated numerical model analyses and directly-observed wind vectors. a) Meteosat IR image on 15 Feb.1997, 0900UTC, superimposed with the CMW vectors with a quality flag QF >1100. b) Collocated wind vectors in the 3-hour forecast from LAM at the same height as that of the corresponding CMW vectors. c) Same as (b) but for ECM 3-hour forecast. d) Collocated directly-observed wind vectors within ±3 hours of 0900UTC at the height closest to the CMW height.

(b) Choice of QF criterion and its ability to discriminate

CMW vectors associated with QF values lower than a specified criterion are taken as unreliable and removed from CWIS outputs before further analysis. Figure 5 represents the relationship between QF values and the accumulated number of CMW vectors(QF > 0 and speed >2.5ms$^{-1}$) for the 5 cases. The maximum value of the QF is between 3000 and 3500. Most vectors are concentrated around QF=2000-2300. QF=1100 is approximately where the derivative of the accumulated number of CMW vectors with respect to QF tends to be zero. So QF =1100 can be taken as a critical value for quality control. Nevertheless, the criterion for QF should be some value reasonably larger than 1100 if a compromise is made between the number of available CMW vectors and the possibility for poor vectors to pass through this quality control.

To test the effectiveness of QF in quality control, comparisons were made between the CMW and the LAM for 3 different QC criteria. The resulting statistics(bias and rms of wind speed and vector differences) are given in Table 2. It can be seen that, as the QF criterion increases from 1100 in steps of 500, RMS differences decrease for every one of the 5 cases at any pressure levels. This proves the capability of QF to discriminate with respect to the quality of CMW vectors. Similar results have also

been obtained from the comparison of CMW with direct observations, which will be described in Section 4d.

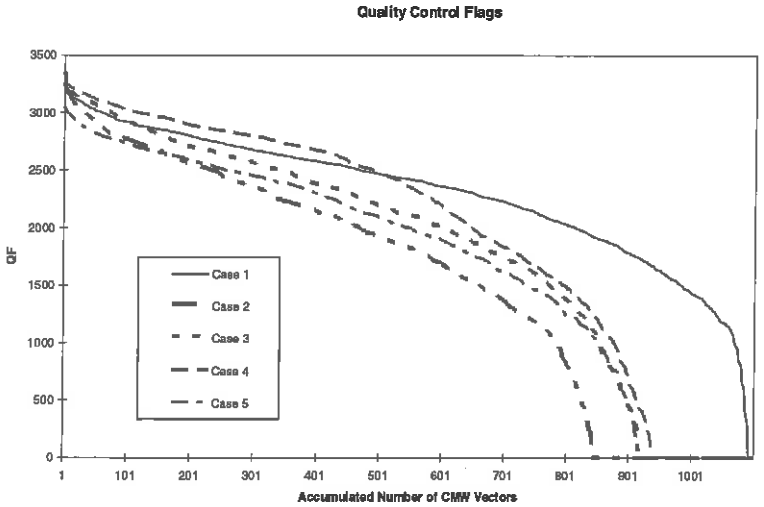


Figure 5. The relationship between QF values and the accumulated number of non-zero(QF>0 and speed>0) CMW vectors for 5 FASTEX Intensive Observing Period cases

TABLE 2. STATISTICS OF CMW VECTORS AS COMPARED WITH LAM ANALYSIS (N=sample size, and other statistics are in unit of $ms^{-1}$. The MEAN_s is the mean speed of CMW.)

| | QF>1100 | | | | | QF>1600 | | | | | QF>2100 | | | | |
|---|---|---|---|---|---|---|---|---|---|---|---|---|---|---|---|
| Level (hPa) | N | MEAN_s | BIAS_s | RMS_s | RMS_V | N | MEAN_s | BIAS_s | RMS_s | RMS_V | N | MEAN_s | BIAS_s | RMS_s | RMS_V |
| *Case_1* | | | | | | | | | | | | | | | |
| 100-1000 | 1688 | 17.2 | -0.7 | 3.2 | 5.1 | 1514 | 16.7 | -0.7 | 3.0 | 4.5 | 1212 | 16.2 | -0.7 | 2.9 | 4.0 |
| 100-400 | 246 | 30.2 | 0.3 | 3.8 | 8.2 | 204 | 28.3 | 0.1 | 3.6 | 7.0 | 144 | 25.6 | -0.3 | 3.3 | 5.4 |
| 401-700 | 723 | 17.2 | -1.6 | 3.7 | 5.4 | 643 | 16.9 | -1.7 | 3.5 | 5.0 | 516 | 16.9 | -1.6 | 3.4 | 4.5 |
| 701-1000 | 719 | 12.8 | -0.1 | 2.3 | 3.1 | 667 | 12.8 | 0.0 | 2.3 | 3.1 | 552 | 13.1 | 0.0 | 2.2 | 2.8 |
| LBF | 1688 | 17.2 | -0.2 | 2.1 | 4.3 | 1514 | 16.7 | -0.2 | 2.0 | 3.7 | 1212 | 16.2 | -0.1 | 1.8 | 3.1 |
| *Case_2* | | | | | | | | | | | | | | | |
| 100-1000 | 1276 | 19.7 | -1.1 | 3.6 | 6.9 | 1037 | 19.7 | -0.9 | 3.2 | 6.2 | 711 | 20.0 | -0.8 | 2.9 | 5.3 |
| 100-400 | 450 | 22.8 | -2.2 | 4.5 | 7.9 | 349 | 22.7 | -1.6 | 3.9 | 6.8 | 224 | 23.4 | -1.0 | 3.2 | 6.0 |
| 401-700 | 649 | 18.8 | -0.6 | 3.1 | 6.4 | 546 | 18.9 | -0.6 | 3.0 | 5.8 | 392 | 19.2 | -0.8 | 2.9 | 5.0 |
| 701-1000 | 177 | 15.4 | -0.4 | 2.7 | 5.8 | 142 | 15.7 | -0.2 | 2.3 | 5.5 | 95 | 15.4 | -0.2 | 2.0 | 4.6 |
| LBF | 1276 | 19.7 | -0.4 | 2.6 | 5.7 | 1037 | 19.7 | -0.2 | 2.2 | 5.0 | 711 | 20.0 | -0.1 | 1.7 | 4.1 |
| *Case_3* | | | | | | | | | | | | | | | |
| 100-1000 | 1311 | 23.0 | -0.5 | 3.7 | 6.8 | 1157 | 22.8 | -0.4 | 3.5 | 6.2 | 851 | 22.0 | -0.5 | 3.3 | 5.6 |
| 100-400 | 473 | 25.6 | -0.8 | 3.9 | 7.0 | 423 | 25.0 | -0.7 | 3.6 | 6.3 | 325 | 23.2 | -0.8 | 3.3 | 5.7 |
| 401-700 | 710 | 21.7 | -0.2 | 3.5 | 6.3 | 646 | 21.6 | -0.2 | 3.4 | 5.8 | 493 | 21.2 | -0.2 | 3.2 | 5.5 |
| 701-1000 | 128 | 20.6 | -1.3 | 3.7 | 8.8 | 88 | 21.2 | -0.4 | 3.0 | 8.1 | 33 | 22.2 | 0.2 | 3.1 | 7.6 |
| LBF | 1311 | 23.0 | -0.2 | 2.7 | 5.9 | 1157 | 22.8 | -0.1 | 2.5 | 5.4 | 851 | 22.0 | -0.2 | 2.3 | 5.0 |
| *Case_4* | | | | | | | | | | | | | | | |
| 100-1000 | 1363 | 24.2 | -0.5 | 2.7 | 7.4 | 1204 | 23.6 | -0.5 | 2.6 | 6.7 | 975 | 22.4 | -0.6 | 2.5 | 6.0 |
| 100-400 | 241 | 27.0 | -0.8 | 3.1 | 8.3 | 205 | 26.9 | -1.1 | 3.1 | 7.5 | 135 | 23.8 | -1.6 | 3.2 | 6.2 |
| 401-700 | 778 | 24.1 | -0.1 | 2.7 | 7.3 | 706 | 23.4 | -0.2 | 2.6 | 6.8 | 587 | 22.3 | -0.2 | 2.5 | 6.1 |

| | | | | | | | | | | | | | | | |
|---|---|---|---|---|---|---|---|---|---|---|---|---|---|---|---|
| 701-1000 | 344 | 22.4 | -1.2 | 2.5 | 7.4 | 293 | 22.0 | -1.0 | 1.9 | 6.2 | 253 | 21.6 | -1.1 | 1.9 | 5.7 |
| LBF | 1363 | 24.2 | 0.4 | 1.9 | 6.7 | 1204 | 23.6 | 0.4 | 1.8 | 6.1 | 975 | 22.4 | 0.4 | 1.6 | 5.5 |
| *Case_5* | | | | | | | | | | | | | | | |
| 100-1000 | 1399 | 21.3 | -0.6 | 3.8 | 7.7 | 1197 | 21.3 | -0.5 | 3.5 | 7.0 | 841 | 20.6 | -0.4 | 3.2 | 6.5 |
| 100-400 | 539 | 24.2 | -1.5 | 4.1 | 8.9 | 455 | 24.6 | -1.1 | 3.6 | 8.0 | 314 | 23.1 | -1.0 | 3.4 | 7.5 |
| 401-700 | 620 | 19.9 | -0.1 | 3.7 | 6.7 | 526 | 19.7 | 0.0 | 3.7 | 6.5 | 354 | 19.4 | 0.2 | 3.2 | 6.0 |
| 701-1000 | 240 | 18.3 | -0.1 | 3.1 | 6.7 | 216 | 18.3 | -0.2 | 2.9 | 6.1 | 173 | 18.4 | -0.5 | 2.8 | 5.5 |
| LBF | 1397 | 21.3 | -0.2 | 2.6 | 6.0 | 1197 | 21.3 | -0.2 | 2.4 | 5.5 | 841 | 20.6 | -0.3 | 2.1 | 5.1 |
| *Total* | | | | | | | | | | | | | | | |
| 100-1000 | 7037 | 20.9 | -0.7 | 3.4 | 6.8 | 6109 | 20.6 | -0.6 | 3.2 | 6.1 | 4590 | 20.0 | -0.6 | 3.0 | 5.5 |
| 100-400 | 1949 | 25.3 | -1.2 | 4.0 | 8.1 | 1636 | 25.0 | -1.0 | 3.6 | 7.2 | 1142 | 23.6 | -0.9 | 3.3 | 6.3 |
| 401-700 | 3480 | 20.4 | -0.5 | 3.3 | 6.5 | 3067 | 20.2 | -0.6 | 3.2 | 6.0 | 2342 | 19.9 | -0.5 | 3.0 | 5.5 |
| 701-1000 | 1608 | 16.6 | -0.5 | 2.7 | 5.7 | 1406 | 16.4 | -0.3 | 2.4 | 5.0 | 1106 | 16.3 | -0.3 | 2.3 | 4.4 |
| LBF | 7037 | 20.9 | -0.1 | 2.4 | 5.7 | 6109 | 20.6 | -0.1 | 2.2 | 5.1 | 4590 | 20.0 | -0.0 | 1.9 | 4.6 |

(c) Comparison between CMW and LAM

Taking all the five cases as a whole sample('Total' in Table 2), one can see that, when QF>1100, the bias of CMW speed(BIAS_s) is -0.7ms$^{-1}$, the RMS speed difference(RMS_s) is 3.4ms$^{-1}$ and the RMS vector difference(RMS_V) is 6.8ms$^{-1}$. The RMS_s and RMS_V decrease to 3.0 and 5.5ms$^{-1}$, respectively, as the QF criterion increases to 2100 though BIAS_s gets slightly closer to zero by 0.1ms$^{-1}$. The RMS direction difference(not given in the table) is 17.6 degrees for QF>1100 and 14.5 degrees when QF>2100. In general, the differences are larger at upper levels(100-400hPa) than at lower levels(701-1000hPa). At the LBF, BIAS_s, RMS_s and RMS_V are -0.1, 2.4 and 5.7 ms$^{-1}$, respectively, for QF>1100 and -0.0, 1.9 and 4.6 for QF>2100.

Statistics for individual cases, given in Table 2, show that the quality of the CMW vectors is consistent between cases despite the detailed differences in cloud type and distributions. Similar to the behaviour in the "Total" statistics, the mean speed and RMS differences increase with height for each case with only one major exception. This is for the low levels in Case 3, in which RMS_V is 8.8ms$^{-1}$, larger than those at high and medium levels by 1.8 and 2.5 ms$^{-1}$, respectively. Since the RMS_s for this case does not show anything abnormal, the large value of RMS_V must be caused by large differences in low-level wind direction between CMW and LAM. Nearly half of the 128 collocated low-level vectors are concentrated in a small area of 5°*5° around 47°N, 47°W, where the CMW

vectors are in the direction of about 275° while the LAM vectors are about 315°. This discrepancy is similar to that shown in Fig.4 for Case 2 as discussed in Section 4c but is situated slightly farther west. According to the satellite imagery at 0900UTC on 17 February, this area is behind a long frontal cloud band and is covered by stable, low cloud which is suitable for tracking. The CMW quality flags in this area are as high as 2500 before assimilation and are still around 2150 even after degradation during assimilation because of the direction difference. Thus we had a reasonable level of confidence in the validity of the CMW vectors in this region even before any direct observations were available for verification. Fortunately, a few buoys and ships were found in this area, showing that the wind was 260°-280° and providing more support to the CMW than to the LAM. The CMW in this region is also supported by the ECM analysis described in the following.

(d) Comparison between CMW and ECM

The ECM 3-hour forecasting were used as an independent data source for comparison with the CMW from the CWIS. For spatial collocation, ECM wind field were interpolated in 3 dimensions according to the geographical co-ordinate and height of CMW vectors(QF>0 and speed>2.5 $ms^{-1}$). The results from the comparison are given in Table 3 in the same form as in Table 2 except that the statistics at the LBF are not available in Table 3. (Note that the sample sizes in Table 3 are also the numbers of available CMW vectors because of the spatial interpolation for collocation. The sample sizes in Table 2 show that CMW vectors was multi-collocated with the LAM by a factor of about 1.6.)

TABLE 3. STATISTICS OF CMW VECTORS AS COMPARED WITH ECMWF 3-HOUR FORECAST
(N=sample size, and other statistics are in unit of $ms^{-1}$. The MEAN_s is the mean speed of CMW.)

| | QF>1100 | | | | | QF>1600 | | | | | QF>2100 | | | | |
|---|---|---|---|---|---|---|---|---|---|---|---|---|---|---|---|
| Level (hPa) | N | MEAN_s | BIAS_s | RMS_s | RMS_V | N | MEAN_s | BIAS_s | RMS_s | RMS_V | N | MEAN_s | BIAS_s | RMS_s | RMS_V |
| *Case_1* | | | | | | | | | | | | | | | |
| 100-1000 | 1063 | 16.8 | -0.1 | 3.2 | 4.4 | 955 | 16.3 | -0.1 | 3.1 | 4.2 | 764 | 16.0 | 0.0 | 2.8 | 3.7 |
| 100-400 | 151 | 28.2 | -1.4 | 4.3 | 6.0 | 126 | 26.4 | -1.3 | 4.3 | 5.8 | 92 | 24.0 | -1.3 | 3.8 | 5.3 |
| 401-700 | 479 | 16.8 | 0.0 | 3.3 | 4.8 | 425 | 16.6 | -0.1 | 3.1 | 4.4 | 343 | 16.4 | 0.0 | 2.8 | 3.9 |
| 701-1000 | 433 | 12.8 | 0.3 | 2.6 | 3.3 | 404 | 12.9 | 0.4 | 2.5 | 3.2 | 329 | 13.3 | 0.4 | 2.3 | 2.8 |
| *Case_2* | | | | | | | | | | | | | | | |
| 100-1000 | 771 | 19.1 | -0.2 | 4.4 | 6.7 | 626 | 18.9 | 0.0 | 4.4 | 6.2 | 426 | 19.1 | 0.1 | 4.2 | 5.9 |
| 100-400 | 255 | 23.1 | -1.4 | 5.0 | 7.9 | 197 | 22.7 | -1.0 | 4.9 | 7.4 | 128 | 23.3 | -0.7 | 4.8 | 7.2 |

| | | | | | | | | | | | | | | | |
|---|---|---|---|---|---|---|---|---|---|---|---|---|---|---|---|
| 401-700 | 416 | 17.8 | 0.5 | 4.3 | 6.2 | 350 | 17.7 | 0.4 | 4.3 | 5.8 | 245 | 18.0 | 0.4 | 4.2 | 5.5 |
| 701-1000 | 100 | 14.4 | 0.3 | 3.4 | 4.1 | 79 | 14.6 | 0.4 | 3.2 | 3.9 | 53 | 14.1 | 0.6 | 2.7 | 3.6 |
| *Case_3* | | | | | | | | | | | | | | | |
| 100-1000 | 845 | 22.2 | -0.7 | 5.9 | 9.1 | 752 | 22.0 | -0.7 | 5.8 | 8.8 | 558 | 21.2 | -0.5 | 5.4 | 8.1 |
| 100-400 | 293 | 23.9 | -3.6 | 7.4 | 12.5 | 263 | 23.5 | -3.7 | 7.5 | 12.1 | 202 | 21.9 | -3.2 | 6.5 | 11.0 |
| 401-700 | 471 | 21.3 | 0.9 | 4.9 | 6.6 | 433 | 21.2 | 1.0 | 4.8 | 6.2 | 331 | 20.8 | 1.1 | 4.7 | 6.0 |
| 701-1000 | 81 | 21.0 | 0.4 | 4.2 | 5.8 | 56 | 21.7 | 0.8 | 3.9 | 5.0 | 25 | 22.2 | 1.7 | 4.3 | 4.9 |
| *Case_4* | | | | | | | | | | | | | | | |
| 100-1000 | 861 | 23.5 | 0.2 | 3.5 | 5.6 | 767 | 23.0 | 0.1 | 3.4 | 5.1 | 623 | 21.8 | 0.1 | 3.4 | 4.8 |
| 100-400 | 159 | 26.1 | 1.5 | 4.3 | 6.6 | 136 | 25.8 | 1.6 | 4.5 | 6.4 | 94 | 22.8 | 2.3 | 4.9 | 6.0 |
| 401-700 | 509 | 23.1 | -0.2 | 3.3 | 5.5 | 465 | 22.5 | -0.2 | 3.2 | 5.2 | 384 | 21.6 | -0.3 | 3.1 | 4.8 |
| 701-1000 | 193 | 22.5 | 0.1 | 3.4 | 5.2 | 166 | 22.0 | 0.0 | 3.1 | 4.0 | 145 | 21.8 | -0.1 | 3.1 | 3.8 |
| *Case_5* | | | | | | | | | | | | | | | |
| 100-1000 | 839 | 21.0 | -0.6 | 4.9 | 8.0 | 707 | 20.9 | -0.4 | 4.5 | 7.6 | 496 | 20.4 | -0.5 | 4.3 | 7.2 |
| 100-400 | 325 | 23.4 | -2.4 | 5.4 | 9.4 | 271 | 23.8 | -2.0 | 4.8 | 8.8 | 191 | 22.8 | -2.1 | 4.8 | 8.9 |
| 401-700 | 386 | 19.8 | 0.2 | 4.8 | 7.4 | 322 | 19.4 | 0.2 | 4.6 | 7.1 | 214 | 19.2 | 0.1 | 4.2 | 6.4 |
| 701-1000 | 128 | 18.4 | 1.7 | 3.7 | 5.5 | 114 | 18.2 | 1.5 | 3.3 | 4.9 | 91 | 18.3 | 1.7 | 3.2 | 4.1 |
| *Total* | | | | | | | | | | | | | | | |
| 100-1000 | 4379 | 20.4 | -0.3 | 4.4 | 6.9 | 3807 | 20.1 | -0.2 | 4.3 | 6.5 | 2867 | 19.5 | -0.1 | 4.0 | 6.0 |
| 100-400 | 1183 | 24.4 | -1.8 | 5.6 | 9.3 | 993 | 24.1 | -1.7 | 5.6 | 9.0 | 707 | 22.8 | -1.5 | 5.2 | 8.6 |
| 401-700 | 2261 | 19.9 | 0.3 | 4.1 | 6.1 | 1995 | 19.6 | 0.3 | 4.0 | 5.8 | 1517 | 19.3 | 0.2 | 3.8 | 5.3 |
| 701-1000 | 935 | 16.5 | 0.5 | 3.2 | 4.4 | 819 | 16.2 | 0.5 | 2.9 | 3.9 | 643 | 16.3 | 0.5 | 2.8 | 3.4 |

It can be seen that the principal feature shown in Table 3 is the same as in Table 2, i.e., the rms speed and vector differences are larger at upper levels and smaller at lower levels, and decrease as the QF criterion increases. Since the CMW vectors were derived completely independently of the ECMWF products, the results given in Table 3 are expected to be worse than those in Table 2. As is seen, the values of BIAS_s fluctuate in a slightly larger range in Table 3 at different heights and for different cases than in Table 2; most of RMS_s values in Table 3 are about 1 $ms^{-1}$ worse than in Table 2; and RMS_V at high levels in Case 3 is as much as 5 $ms^{-1}$ worse. However, in "Total" for all levels, BIAS_s is 0.4 $ms^{-1}$ better, and RMS_s and RMS_V are 4.4 and 6.9 $ms^{-1}$, respectively, at QF>1100, i.e., not too far from 3.4 and 6.8 $ms^{-1}$ in Table 2. In addition, the statistics show that the CMW fields for Cases 1 and 4 are generally closer to the ECM than to the LAM, and that rms vector differences between CMW and ECM at low levels for Cases 2, 3 and 5 are better than between CMW and LAM. This is especially so for Case 3 at low levels, for which RMS_V in Table 3 is 3 $ms^{-1}$ better than in Table 2. In summary, if the sum of RMS_s and RMS_V is used as an overall measure of closeness of fit, CMW fields are closer to LAM analyses at high and medium levels and to ECM analyses at low levels.

Comparison has been made at ECMWF between the ECM 6-hour forecasts and CMWs generated by satellite-operating countries and organisations(Tomassini et al. 1997). Statistics of CMW vectors from IR images for the area 20°N-90°N during the period October 1996 - December 1996 are given in Table 4. The corresponding results from the present study with respect to both the ECM and LAM 3-hour predictions are also summarised in Table 4. It can be seen that the results from the present study are comparable with those obtained by other researchers.

TABLE 4. STATISTICS OF CMWS RECEIVED AT ECMWF FOR DIFFERENT SATELLITES DURING THE PERIOD OCTOBER 1996 - DECEMBER 1996 WITH RESPECT TO NUMERICAL WEATHER PREDICTION(Tomassini et al. 1997) AND STATISTICS FROM THE PRESENT STUDY
(The values of MEAN_s from Tomassini et al.(1997) are the mean speed of NWP, while the values of MEAN_s from the present study are the mean speed of CMW.)

| | | High level | | | Medium level | | | Low level | | |
|---|---|---|---|---|---|---|---|---|---|---|
| Satellite | NWP Model | MEAN s | BIAS s | RMS V | MEAN s | BIAS s | RMS V | MEAN s | BIAS s | RMS V |
| | | *Tomassini et al. (1997):* | | | | | | | | |
| GOES-8 | ECM | 22.3 | -1.6 | 5.6 | 13.0 | -0.9 | 4.8 | 8.9 | -0.5 | 3.8 |
| GOES-9 | ECM | 25.0 | -1.7 | 6.0 | 15.2 | -0.8 | 5.0 | 10.6 | -0.3 | 3.6 |
| Meteosat | ECM | 27.5 | -2.3 | 7.7 | 17.4 | -1.7 | 6.1 | 9.9 | -0.3 | 2.9 |
| GMS | ECM | 31.1 | -2.7 | 8.7 | | | | 8.6 | 0.1 | 3.3 |
| | | *The present study at QF>1100* : | | | | | | | | |
| Meteosat | ECM | 24.4 | -1.8 | 9.3 | 19.9 | 0.3 | 6.1 | 16.5 | 0.5 | 4.4 |
| | LAM | 25.3 | -1.2 | 8.1 | 20.4 | -0.5 | 6.5 | 16.6 | -0.5 | 5.7 |
| | | *The present study at QF>2100* : | | | | | | | | |
| | ECM | 22.8 | -1.5 | 8.6 | 19.3 | 0.2 | 5.3 | 16.3 | 0.5 | 3.4 |
| | LAM | 23.6 | -0.9 | 6.3 | 19.9 | -0.5 | 5.5 | 16.3 | -0.3 | 4.4 |

(e) Comparison with direct observations

Direct observations are potentially the most appropriate data to be used for verification, but their availability is limited even in the present study. All the direct observations made by both dropsondes from UK and US research aircraft and radiosondes from observing ships and conventional sounding stations are becoming available for FASTEX studies. However, it is still difficult to get a satisfactory number of CMW vectors collocated with direct observations for statistical comparisons. Most of the wind data from dropsondes used in this study are from the UK C 130 and they are concentrated between 450 and 900 hPa in the vertical and in a small area in the horizontal. Only Case 2, shown in

Fig.4, benefits from US Gulfstream-IV dropsondes because it was not releasing dropsondes for the other cases at the time when the UK C 130 was operating. Wind data from the Gulfstream-IV dropsondes start at about 340hPa. Each radiosonde launching station on ground and observing ships made a launch about every 3 or 6 hours. Therefore, to achieve a sufficient number of collocated observations, the time criterion for the difference between CMW and sondes is set as large as 3 hours even though the locations differ by no more than 0.5 ° latitude and 1 ° longitude. A height difference of 100hPa is used as the criterion in the vertical. Sea-surface wind data from buoys and ships are used for low-level wind comparison if they can be collocated under the same definition for collocation in 4 dimensions as described above. The comparison is completed by taking all 5 cases together as a total and the result is given in Table 5.

TABLE 5. RESULTS FROM THE COMPARISONS OF CMW WITH DIRECT OBSERVATIONS
(N is the number of vectors compared, and other statistics are in unit of $ms^{-1}$.
The values of MEAN_s are the mean speed of CMW, ECM and LAM, respectively.)

| | Level(hPa) | N | MEAN_s | BIAS_s | RMS_s | RMS_V |
|---|---|---|---|---|---|---|
| CMW | | | *QF>1100:* | | | |
| | 100-1000 | 257 | 22.2 | 0.1 | 5.6 | 9.4 |
| | 100- 400 | 76 | 31.9 | 1.5 | 5.7 | 8.4 |
| | 401- 700 | 126 | 19.6 | -0.9 | 5.8 | 10.1 |
| | 701-1000 | 55 | 14.5 | 0.4 | 5.1 | 9.0 |
| | LBF | 245 | 23.9 | -0.1 | 3.5 | 7.3 |
| | | | *QF>1600:* | | | |
| | 100-1000 | 220 | 21.2 | 0.4 | 5.5 | 8.3 |
| | 100- 400 | 69 | 30.2 | 1.4 | 5.6 | 8.2 |
| | 401- 700 | 105 | 18.2 | -0.4 | 5.7 | 8.3 |
| | 701-1000 | 46 | 14.7 | 0.8 | 4.7 | 8.5 |
| | LBF | 201 | 22.3 | -0.3 | 2.5 | 5.5 |
| | | | *QF>2100:* | | | |
| | 100-1000 | 130 | 19.2 | 0.5 | 4.8 | 7.3 |
| | 100- 400 | 40 | 25.1 | 1.0 | 5.3 | 8.1 |
| | 401- 700 | 64 | 17.0 | -0.2 | 4.9 | 6.9 |
| | 701-1000 | 26 | 15.2 | 1.5 | 3.6 | 6.6 |
| | LBF | 114 | 19.9 | -0.3 | 2.1 | 4.1 |
| LAM | 100-1000 | 12138 | 25.8 | -0.2 | 5.7 | 9.5 |
| | 100- 400 | 3369 | 35.2 | 0.7 | 5.6 | 10.6 |
| | 401- 700 | 4013 | 26.7 | -0.5 | 5.5 | 8.8 |
| | 701-1000 | 4756 | 18.3 | -0.7 | 5.9 | 9.3 |
| ECM | 100-1000 | 315 | 21.9 | -0.5 | 7.2 | 9.6 |
| | 100- 400 | 79 | 32.8 | 2.2 | 6.5 | 10.9 |
| | 401- 700 | 136 | 19.8 | -1.1 | 8.0 | 9.9 |
| | 701-1000 | 100 | 16.3 | -1.8 | 6.4 | 8.2 |

The difference in sample size, N, at 3 different levels, as seen in Table 5, reflects the height characteristics of the directly observed data. Roughly half the compared vectors are at the medium levels(401-700hPa) because of the availability of large number of UK C 130 dropsondes at or near the reference time. The other half, distributed in the upper (above 400hPa) and lower (under 701hPa) levels, are mainly from radiosondes and the US Gulfstream-IV dropsondes for the upper levels and from buoys for the low levels.

The main results from Table 5 are:

(i) BIAS_s is always less than 1.5ms $^{-1}$ at all levels and is no more than 0.5 ms $^{-1}$ on average;

(ii) RMS_s increases with height in line with the mean speed;

(iii) RMS_V increases markedly with height for QF>2100, and decreases negligibly if QF>1600. When QF>1100, RMS_V at medium levels is as large as 10.1ms $^{-1}$ but this is only because a single CMW vector at 55.68 $^{\circ}$ N, 17.29 $^{\circ}$ W in CASE 3 has a large difference in wind direction as compared with the dropsondes around it. Since it has a low QF value of 1388, increasing the QF criterion would effectively decrease RMS_V as is seen for QF>1600;

(iv) As QF criterion increases, RMS_s and RMS_V decrease.

Because the clouds in the dropsonde areas are convective or multilayered and the dropsondes were released in dynamically active regions where winds are often varying rapidly with time, the cloud tracking and height assignment are made more difficult. Taking this into account the results in Table 5 are quite encouraging. Compared with the monthly RMS vector difference of CMW winds versus radiosonde winds(Woick 1996), the RMS_V in Table 5 for QF>1600 is about 1ms $^{-1}$ better at the upper levels, 1ms $^{-1}$ worse at medium levels, and 3ms $^{-1}$ worse at lower levels.

Another factor that degrades the quality of the above results is the looseness of the 3-hour time criterion for acceptance of observations in the comparisons. This is especially so in the areas of strong wind gradients around the major cyclone observed in the study. To evaluate the sensitivity to this, comparisons between CMW vectors and dropsondes have also been carried out using the UK C 130

observations for Case 4 displaced horizontally by an amount that takes into account the time difference and the movement of the cyclone system during that time, as was done in a study by Browning et al.(1995). The results of this test are given in Table 6. At medium levels where most of the compared vectors are concentrated, both RMS_s and RMS_V improve by 0.5 and 1.4 $ms^{-1}$, respectively, though BIAS_s increases by 0.8 $ms^{-1}$. The representativeness of the statistics at upper and low levels is adversely affected by sample size. For the particular adjustment procedure used, the speed of the weather system was biased towards the lower atmosphere. This implies that the improvement of RMS_V at lower levels should be greater than at upper levels. Despite the very small sample size at high and low levels, the increase of RMS_V at upper levels and its marked decrease at low levels, shown in Table 6, are qualitatively consistent with expectation. In general, the displacement of the dropsondes makes the rms direction difference decrease from 29.5° to 21.2°(not given in the table) and RMS_V decrease by 1.9$ms^{-1}$. This implies that the quality of the CWIS vectors given in Table 5 is slightly underestimated.

TABLE 6. IMPACT OF HORIZONTAL DISPLACEMENT OF DROPSONDES ON VERIFICATION OF CMW FOR CASE 4(QF>1100)

| | Before adjustment | | | | | After adjustment | | | | |
|---|---|---|---|---|---|---|---|---|---|---|
| Level(hPa) | N | MEAN_s | BIAS_s | RMS_s | RMS_V | N | MEAN_s | BIAS_s | RMS_s | RMS_V |
| 100-1000 | 45 | 21.0 | 0.2 | 6.1 | 9.8 | 48 | 23.8 | 0.8 | 5.7 | 7.9 |
| (100- 400 | 8 | 40.2 | 1.4 | 4.1 | 5.8 | 15 | 38.1 | 0.6 | 5.0 | 7.3)* |
| 401- 700 | 33 | 16.8 | 0.3 | 6.6 | 9.6 | 31 | 17.5 | 1.1 | 6.1 | 8.2 |
| (701-1000 | 4 | 17.0 | -2.8 | 5.1 | 15.5 | 2 | 14.0 | -2.0 | 4.5 | 7.8) |
| LBF | 46 | 21.4 | -0.7 | 2.7 | 7.1 | 48 | 23.8 | 0.0 | 2.7 | 4.9 |

* Brackets indicate low confidence owning to very small sample size.

A comparison of numerical analyses from LAM and ECM with all directly observed data is also given in Table 5. One can see that CMW quality at QF>1100 is generally equivalent to the quality of both LAM and ECM; indeed it is better when QF>1600 and even better at all levels as QF increases further even though the mean speed does not decrease very much. It also seems rational for the CMW fields to be closer to the LAM analyses at high and medium levels and to the ECM analyses at low levels, which was summarized in the last sub-section,

## 5. CONCLUSIONS

An auto-adapting tracking technique, independent of the first guess to the wind field, is designed to extract cloud motion vectors from geostationary satellite images. The auto-adapting scheme, which simulates a blind person finding his way to the top of a hill, improves the computing efficiency. It has been implemented as a PC-based experimental cloud-motion wind-inferring system.

The system uses a pattern recognition parameter couple, which consists of both the central moment correlation coefficient and the original moment correlation coefficient. This is to be compared with most of the current operational systems in which only a single parameter is used for pattern recognition. An accompanying automated consistency analysis is performed and quality flags are marked with a cross-checking scheme specially designed for processing a quartet of raw CMW field derived from a satellite imagery triplet with the pattern recognition parameter couple. These procedures increase the cloud motion information and its reliability.

The comparison of the cloud motion vectors with the analyses(and 3-hour forecast) from the UKMO LAM model, whose 12-hour forecasts were used during CMW height assignment through assimilation, shows that the bias and rms speed difference and the rms vector difference are, respectively, -0.7, 3.4 and 6.8 $ms^{-1}$ for a criterion-of-quality flag QF=1100. As QF increases up to 2100, the sample size decreases from 7037 to 4590(correspondingly, the total number of available cloud motion vectors decreases from 4379 to 2867, i.e., ~65%) and the bias and rms speed difference, and the rms vector difference decrease to -0.6, 3.0 and 5.5 $ms^{-1}$, respectively.

Comparison with the 3-hour forecasts from the ECMWF model, which CMW is independent of, shows that the RMS_s and RMS_V are slightly worse (by less than 1 $ms^{-1}$) in general, but it appears that CMW fields are closer to ECMWF 3-hour forecasts at low levels and to LAM model analysis(and 3-hour forecasts) at high and medium levels in terms of the sum of RMS_s and RMS_V. This is

supported by the comparison of model analyses with direct observations. The statistics from the comparisons of CMW with LAM and ECM analyses are consistent with those obtained by other researchers.

The comparison of CMW with direct observations from dropsondes, radiosondes, buoys and ships, shows that, given QF>1600, the bias and rms speed differences and rms vector difference are 0.4, 5.5 and 8.3 $ms^{-1}$, respectively, which are better than numerical model analysis. It is shown that these values, representing the quality of CMW vectors, can be further improved by adjusting the non-time-sychronous observations according to the velocity of weather systems.

Further work is suggested to carry out experiments, if possible, on one of the current operational CMW systems in comparison with the technique described in this paper. This would enable a complete, quantitative evaluation to be made of the computing efficiency, the amount of cloud motion information and its accuracy and reliability within the same program-running and data-accessing environment, in a larger area and with more direct observations.


## ACKNOWLEDGEMENTS

This research was carried out at the Joint Centre for Mesoscale Meteorology, University of Reading, whilst Wang Zhenhui was in receipt of a Sino-British Friendship Scholarship. We are grateful to Peter Panagi for considerable assistance in the provision of model and satellite data and to Ray Saktreger for help with the PC computer.

We wish to thank the many participants in the FASTEX experiment for the rich variety of data used for validation and in particular Meteo-France for access to the Central Archive for FASTEX established in Toulouse. We especially thank members of the UK Met Office for early provision of high-resolution dropsonde data from the UK C 130 aircraft, especially Sid Clough, Andy Macallan and Tim Hewson. Also we like to thank Micheal Rohn of ECMWF for helpful advice.

Wang Zhenhui would also like to give his particular thanks to JCMM and the Department of Meteorology, University of Reading, for providing him with the research facilities used during his stay.

## REFERENCES

Browning, K. A., Clough, S. A., Davitt, C. S. A., Robert, N. M., Hewson, T. D., and Healey, P. G. 1995: Observations of the mesoscale sub_structure in the cold air of a developing frontal cyclone. *Q. J. R. Meteorol. Soc.*, **121**, 1229-1254.

Buhler,Y. and Holmlund, K. 1993: The Cloud Motion Wind Extraction Algorithm for MTP/MPEF. *Proceedings to Second International Wind Workshop*, in Tokyo, Japan, 13-15 Dec. 1993, 205-217.

Cullen, M. J. P. 1993: The unified forecast climate model. *Meteorol. Mag.*, **122**, 81-94.

Dent, D. W., 1993: Parallelization of the IFS model. In "Parallel supercomputing in atmospheric science" edited by G. R. Hoffmann and T. Kauranne. World Scientific Publishing Co., Singapore. 532pp.

Hayden, C. M. 1993: Recent Research in the Automated Quality Control of Cloud Motion Vectors at CIMSS/NESDIS. *Proceedings to Second International Wind Workshop*, in Tokyo, Japan, 13-15 Dec. 1993, 219-226.

Holmlund, K. 1993: Operational Water Vapor Wind Vectors from Meteosat Imagery Data. *Proceedings of Second International Wind Workshop*, in Tokyo, Japan, 13-15 Dec. 1993, 77-84.

Holmlund, K. 1996: Normalized Quality Indicators for Eumetsat Cloud Motion Winds. *Proceedings to the Third International Wind Workshop*, in Ascona, Switzerland, 10-12 June 1996, 155-164.

Joly ,A.., Jorgensen, D., Shapiro,M. A., Thorpe A. J., Bessemoulin, P., Browning, K. A., Cammas, J. P., Chalon, J. P., Clough, S. A., Emanuel, K. A., Eymard, L., Gall, R., Hildebrand, P. H., Langland, R. H., Lemaitre, Y., Lynch, P., Moore, J. A., Persson, P. O. G., Snyder, C. and Wakimoto, R. M. 1997: the Fronts and Atlantic Storm-Track Experiment(FASTEX): Scientific objectives and experimental design. *Bull. Amer. Meteor. Soc.* To appear shortly.

Kelkar, R. R., Rao, A. V. R. K. and Bhatia, R. C. 1993: Resent Improvement in Cloud Motion Vector Derivation from INSAT. *Proceedings to Second International Wind Workshop*, in Tokyo, Japan, 13-15 Dec. 1993, 65-70.

Kelly, G. 1997: Influence of observations on the operational ECMWF system. *ECMWF Newsletter*. **76**, 2-7.

Marshall, J. L., Pescool, N., Seaman, B., Mills, G. and Stewart, P. 1994: An Operational System for Generating Cloud Drift Winds in the Australian Region and Their Impact on Numerical Weather Prediction. *Weather and Forecasting*. **9**, 361-370.

Menzel, W. P., Wanzong, S., Nieman, S., and Schmetz, J. 1993: Assigning Heights to Cloud Motion Vectors. *Proceedings to Second International Wind Workshop*, in Tokyo, Japan, 13-15 Dec. 1993, 105-115.

Schmetz, J., Holmlund, K., Hoffman, J., Struses, B., Mason, B.,Gaertner, V., Koch, A., and De Berg, L. V., 1993: Operational Cloud Motion Winds from Meteosat Infrared Images. *J. Appl. Meteor.*, **32**, 1206-1225.

Smith, W. L. 1991: A short summary for Panel Discussion. *Proceedings of Workshop on Wind Extraction from Operational Meteorological Satellite Data*, in Washington, D.C., 17-19 Sept. 1991, 6-7.

Takata, S. 1993: Current Status of GMS Wind and Operational Low-level Wind Derivation in a Typhoon Vicinity from Short-time Interval Images. *Proceedings to Second International Wind Workshop*, in Tokyo, Japan, 13-15 Dec. 1993, 29-36.

Tomassini, M., Kelly, G. and Saunders, R. 1997: Use and imapct of satellite atmospheric motion winds on ECMWF analyses and forecasts. *EUMETSAT/ECMWF Research Report* No.6, 1997.

Velden, C. S., Hayden, C. M., Nieman, S. J., Menzel, W. P., Wanzong, S., and Goerss, J. S. 1997: Upper-Troposphric Winds Derived from Geostationary Satellite Water Vapor Observations. *Bull. Ameri. Meteor. Soc.*, **78**, 173-195.

Walter, R. J. Jr. 1993: Current Status of the Operational Wind Extraction Program in NOAA/NESDIS. *Proceedings to Second International Wind Workshop*, in Tokyo, Japan, 13-15 Dec. 1993, 43-43.

Wang Zhenhui and Zeng Weilin. 1996: A PC-based Objective Inferring System for Cloud Motion Winds from Geostationary Satellite Images. *J. Nanjing Institute of Meteorology*, **19**,69-75.

Wang Zhenhui, Tang Dazhang and Fu Desheng. 1991: An Experiment Study on the Pattern Recognition Parameters in Image Processing. *Proceedings of the 16th Conference on Local Severe Storm*, in Canada, 1991, pp?.

Woick, H. 1996: Verification of METEOSAT Wind from MPEF and MIEC. *Proceedings to the Third International Wind Workshop*, in Ascona, Switzerland, 10-12 June 1996, 207-214.

Fig 4a

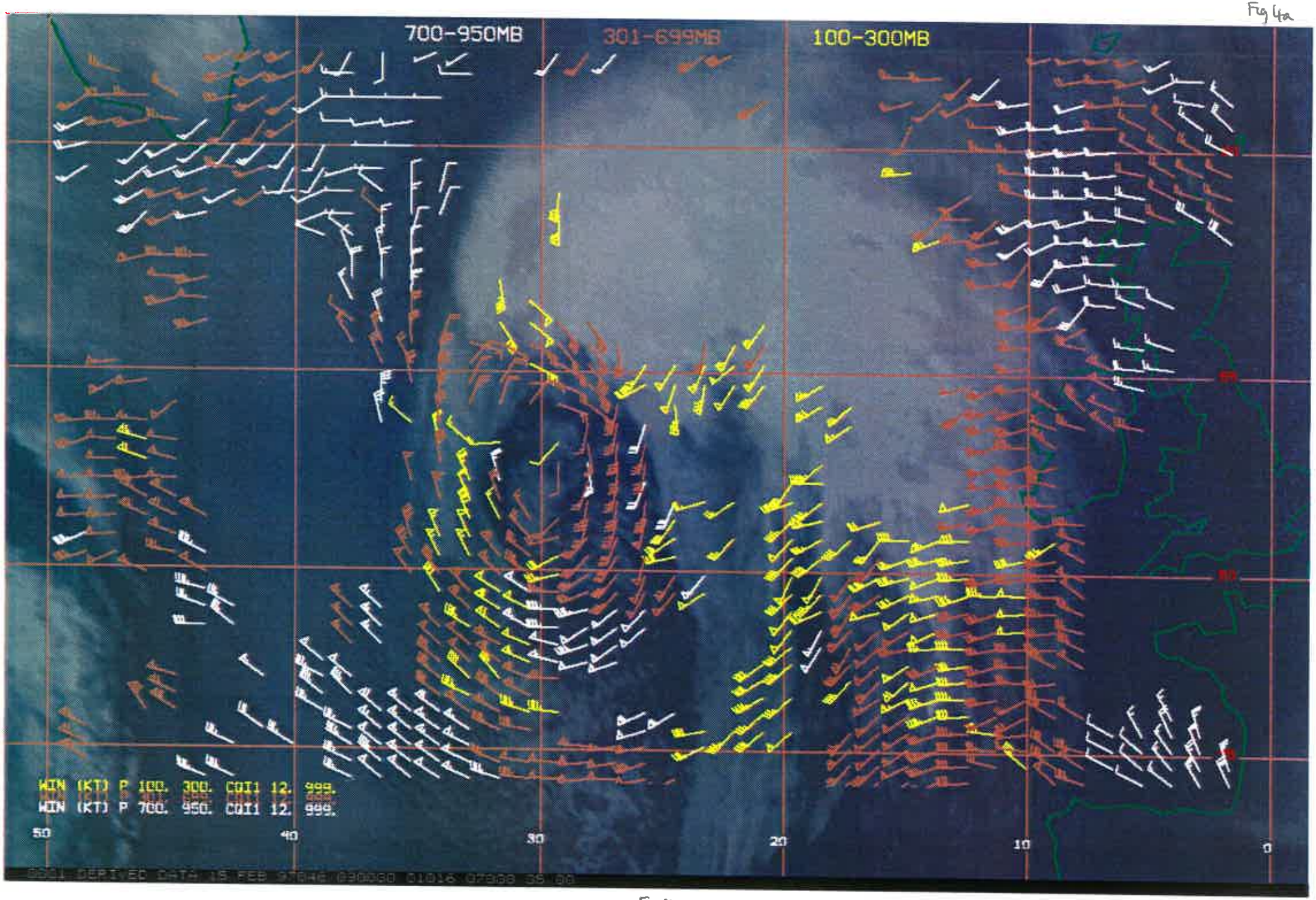
700-950MB
301-699MB
100-300MB
WIN (KT) P 100. 300. COI1 12. 999.
WIN (KT) P 700. 950. COI1 12. 999.
50
40
30
20
10
0

Fig 4a

Fg 4b

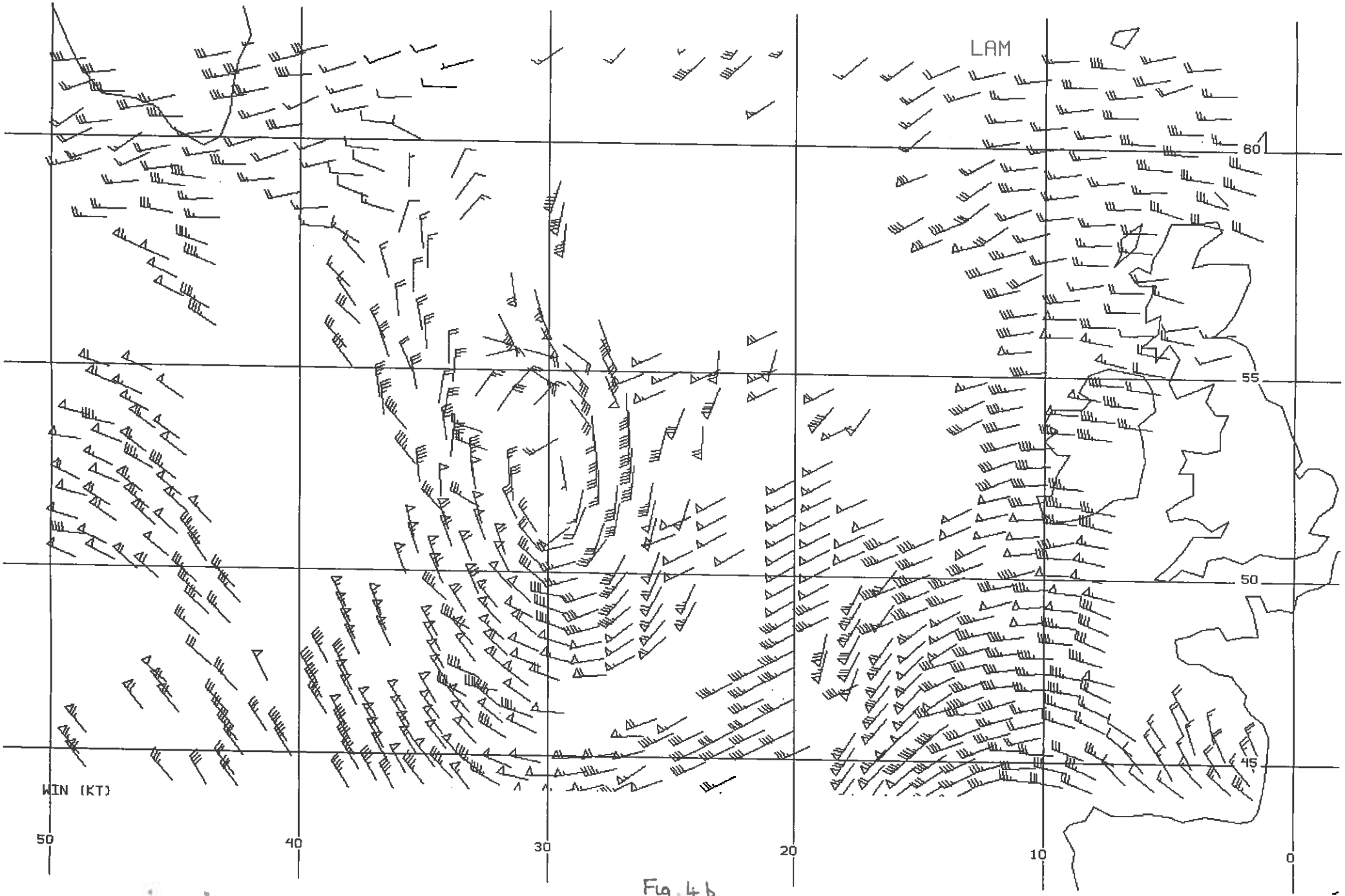


Fig. 4b

Fig4c

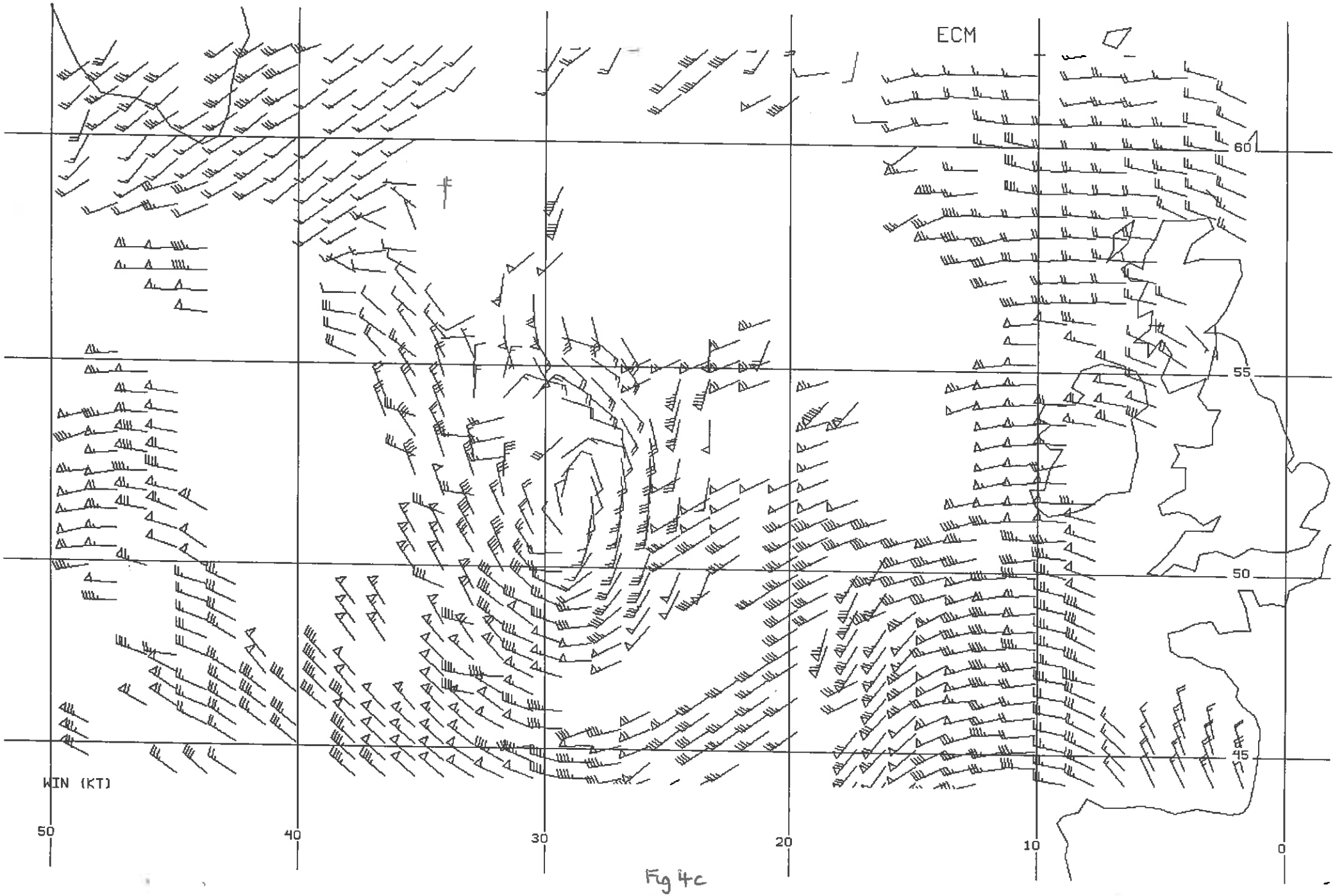


Fig 4c

Fig 4d

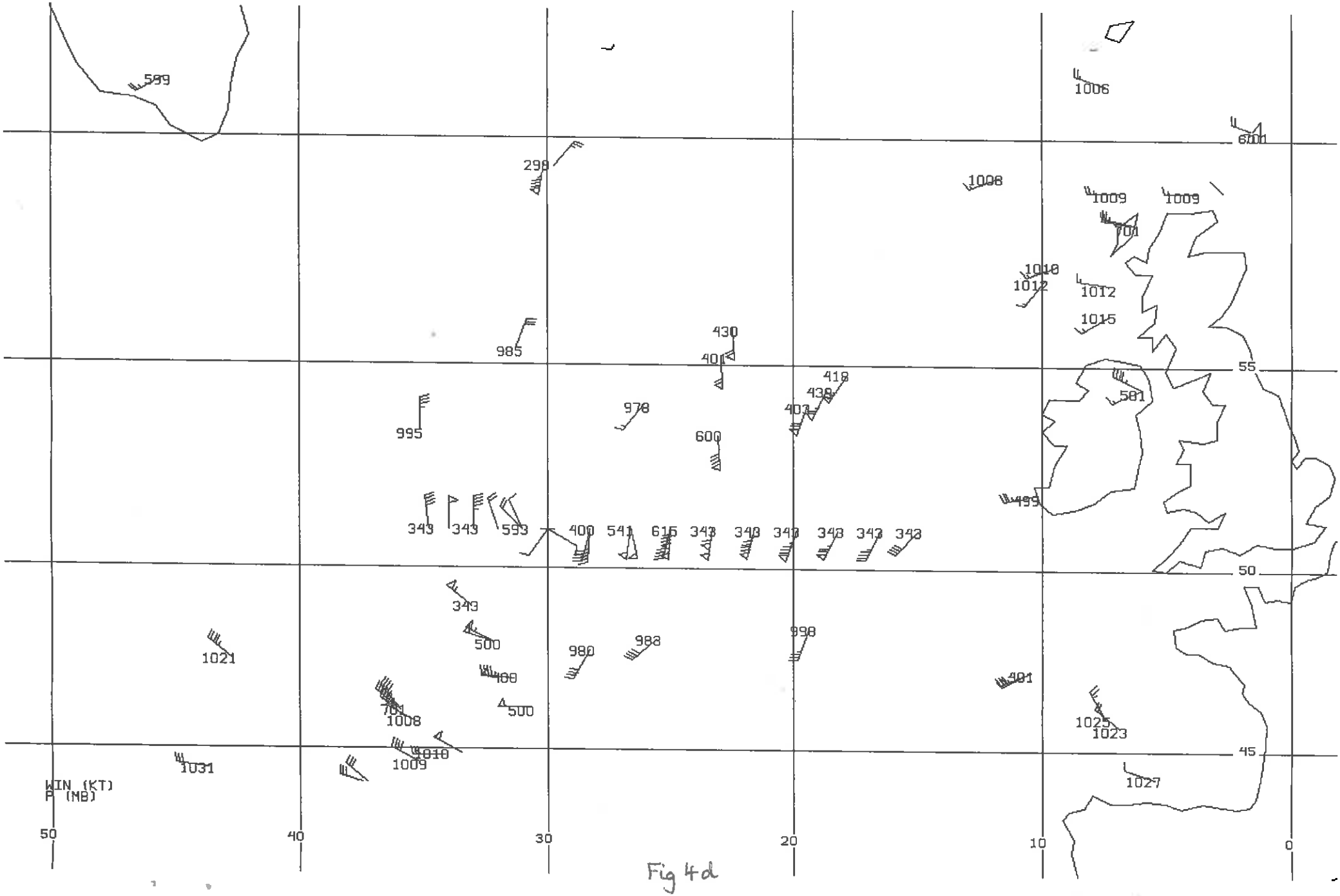

599
298
985
995
978
430
401
600
418
438
407
1006
601
1008
1009
1009
701
1010
1012
1012
1015
501
499
343
343
593
400
541
615
343
343
343
343
343
343
343
500
980
983
998
1021
400
500
701
1008
1010
1009
1031
401
1025
1023
1027
WIN (KT)
P (MB)
55
50
45
50
40
30
20
10
0


Fig 4d

## CURRENT JCMM INTERNAL REPORTS

This series of JCMM Internal Reports, initiated in 1993, contains unpublished reports and also versions of articles submitted for publication. The complete set of Internal Reports is available from the National Meteorological Library on loan, if required.

1. **Research Strategy and Programme**
   K A Browning et al
   January 1993

2. **The GEWEX Cloud System Study (GCSS)**
   **GEWEX Cloud System Science Team**
   January 1993

3. **Evolution of a mesoscale upper tropospheric vorticity maximum and comma cloud from a cloud-free two dimensional potential vorticity anomaly**
   K A Browning
   January 1993

4. **The Global Energy and Water Cycle**
   K A Browning
   July 1993

5. **Structure of a midlatitude cyclone before occlusion**
   K A Browning and N Roberts
   July 1993

6. **Development in Systems and Tools for Weather Forecasting**
   K A Browning and G Szejwach
   July 1993

7. **Diagnostic study of a narrow cold frontal rainband and severe winds associated with a stratospheric intrusion**
   K A Browning and R Reynolds
   August 1993

8. **Survey of perceived priority issues in the parametrizations of cloud-related processes in GCMs**
   K A Browning
   September 1993

9. **The Effect of Rain on Longwave Radiation**
   I Dharssi
   September 1993

10. **Physical Cloud Microprocesses - A Description of the Parametrization used in the Large Eddy Model**
    H Swann
    July 1994

11. **An Appreciation of the Meteorological Research of Ernst Kleinschmidt**
A J Thorpe
May 1992

12. **Potential Vorticity of Flow Along the Alps**
A J Thorpe, H Volkert and Dietrich Heimann
August 1992

13. **The Representation of Fronts**
A J Thorpe
January 1993

14. **A Parametrization Scheme for Symmetric Instability: Test for an Idealised Flow**
C S Chan and A J Thorpe
February 1993

15. **The Fronts 92 Experiment: a Quicklook Atlas**
Edited by T D Hewson
November 1993

16. **Frontal wave stability during moist deformation frontogenesis**
**Part 1. Linear wave dynamics**
C H Bishop and A J Thorpe
May 1993

17. **Frontal wave stability during moist deformation frontogenesis**
**Part 2. The suppression of non-linear wave development**
C H Bishop and A J Thorpe
May 1993

18. **Gravity waves in sheared ducts**
C Bishop and A J Thorpe
November 1993

19. **Potential Vorticity and the Electrostatics Analogy: Quasi-Geostrophic Theory**
C Bishop and A J Thorpe
November 1993

20. **Recent Advances in the Measurement of Precipitation by Radar**
A J Illingworth - April 1993

21. **Micro-Physique et Givrage. Cloud Microphysics and Aircraft Icing**
A J Illingworth May 1993

22. **Differential Phase Measurements of Precipitation**
M Blackman and A J Illingworth
May 1993

23. **Estimation of Effective Radius of Cloud Particles from the Radar Reflectivity**
N I Fox and A J Illingworth
May 1993

24. **A Simple Method of Dopplerising a Pulsed Magnetron Radar**
A Hau, A J Illingworth and J Eastment
November 1993

25. **Radiation and Polar Lows**
George C Craig
February 1994

26. **Collected preprints submitted to the International Symposium on the Life Cycles of Extratropical Cyclones; Bergen, Norway, 27 June - 1 July 1994**
April 1994

27. **Convective Frontogenesis**
Douglas J Parker and Alan J Thorpe
April 1994

28. **Improved Measurement of the Ice Water Content in Cirrus Using a Total Water Evaporator**
Philip R A Brown and Peter N Francis
April 1994

29. **Mesoscale Effects of a Dry Intrusion within a Vigorous Cyclone**
K A Browning and B W Golding
April 1994

30. **GEWEX Cloud System Study, Science Plan**
May 1994

31. **Parametrization of Momentum Transport by Convectively Generated Gravity Waves**
R Kershaw
February 1995

32. **Mesoscale Modelling Newsletter No 5**
May 1994

33. **Observations of the mesoscale sub-structure in the cold air of a developing frontal cyclone**
K A Browning, S A Clough, C S A Davitt, N M Roberts and T D Hewson
May 1994

34. **Longwave Radiative Forcing of a Simulated Tropical Squall Line**
Imtiaz Dharssi
July 1994

35. **On the nature of the convective circulation at a kata-cold front**
K A Browning
September 1994

36. **Collective preprints of papers submitted to the COST-75 International Seminar on Advanced Weather Radar Systems, Brussels, 20-23 September 1994**
November 1994

37. **Use of satellite imagery to diagnose events leading to frontal thunderstorms: Parts 1 and 11 of a case study**
K A Browning and N M Roberts
November 1994

38. **The role of spaceborne millimetre-wave radar in the global monitoring of ice cloud**
P R A Brown, A J Illingworth, A J Heymsfield, G M McFarquahar, K A Browning and M Gosset
December 1994

39. **Potential Vorticity Inversion**
Michael Ziemianski
October 1994

40. **Theory of mature tropical cyclones; a comparison between Kleinschmidt (1951) and Emanuel (1986)**
Suzanne L Gray
December 1994

41. **Dispersion and removal of pollutants during the passage of an atmospheric frontal System**
N R Gimson
December 1994

42. **The role of snow sublimation in frontogenesis**
D J Parker and A J Thorpe
December 1994

43. **Potential vorticity and the electrostatics Analogy: Ertel- Rossby formulation**
A J Thorpe and C H Bishop
December 1994

44. **Mesoscale aspect of extratropical cyclones: an observational perspective**
K A Browning
January 1995

45. **A Polar Low Outbreak: Evolution and Mesoscale Structures**
T D Hewson, G C Craig and C Claud
February 1995

46. **Generation of near-surface gusts of deep convection**
K Nakamura and R Kershaw
April 1995

47. **Attribution Concepts applied to the Omega Equation**
S A Clough, C S A Davitt and A J Thorpe
June 1995

48. **Parametrization of mixed-phase cloud and precipitation**
Susan P Ballard and M Gerard Hutchinson
June 1995

49. **Short-range forecasting of stratocumulus: Initialization Prediction**
Susan Ballard, Simon D Jackson and B Macpherson
June 1995

50. **Contributions of the JCMM/Dept of Meteorology Radar Group to the 27th AMS Radar Meteorology Conference, Vail October 1995**
June 1995

51. **Cold Pools in Shear**
Douglas J Parker
September 1995

52. **High-resolution analysis of frontal fracture**
K A Browning, S P Ballard and C S A Davitt
September 1995

53. **The Albedo of Broken Cloud Fields: Calculations using a modified two stream radiation code**
Imtiaz Dharssi and Roy Kershaw
October 1995

54. **Parametrization of momentum transport by convection. I: Theory and cloud modelling results**
P Kershaw and D Gregory
November 1995

55. **Variation of frontal structure along a cold front**
K A Browning and N M Roberts
November 1995

56. **Secondary Frontal Waves**
Douglas Parker
December 1995

57. **Objective Fronts**
T D Hewson
March 1996

58. **Mesoscale analysis of the activation of a cold front during cyclogenesis**
K A Browning, N M Roberts and A J Illingworth
June 1996

59. **Investigation of Different Representations of Rain in a 1-d Evaporation Model**
H Swann
May 1996

60. **Parametrization of diabatic processes in the inversion of the omega-equation**
M Athanassiadou and A J Thorpe

61. **The Role of the Environmental Flow in the Development of Secondary Frontal Cyclones**
I A Renfrew, A J Thorpe and A Joly
June 1996

62. **Consequences of the geostrophic momentum approximation on barotropic instability**
S Malardel, A J Thorpe and A Joly
June 1996

63. **Contributions to the AMS/RMS Conference on Mesoscale Processes**
Reading, 9-13 September 1996

64. **Vorticity and Potential Vorticity in Stratified Flows Interacting with an Isolated Obstacle**
Jorge A Gutierrez and A J Thorpe
September 1996

65. **Triple Point Development: Two Case Studies**
Douglas Parker
September 1996

66. **Radar observations of wind-shear splitting within evolving atmospheric Kelvin-Helmholtz billows**
D Chapman and K A Browning
April 1997

67. **Cold Frontal Structure derived from radar wind profilers**
K A Browning, D Jerrett, J Nash, T Oakley, N M Roberts
May 1997

68. **The dry intrusion and its effect on the frontal, cloud and precipitation structure of extratropical cyclones**
K A Browning - Text of invited special lecture at the Spring Conference of the Meteorological Society of Japan, University of Tsukuba, 22 May 1997

69. **Met. Office Unified Model data, diagnostic graphics programs, and other observational data available from the JCMM through the aegis of the Universities Weather Research Network UWERN.** Plus supplement.
Peter Panagi and Ed Dicks
June 1997

70. **Contributions of the JCMM/Dept of Meteorology Radar Group to 28th AMS Radar Meteorology Conference.** Austin, Texas, September 1997

71. **Sensitivity of short-range weather forecasts to local potential vorticity modifications**
Meral Demirtas and Alan Thorpe
July 1997

72. **Objective identification of frontal wave cyclones**
T D Hewson
August 1997

73. **Attribution and its application to mesoscale structure associated with tropopause folds**
A J Thorpe
September 1997

74. **The Role of the Environmental Flow in the Development of Secondary Frontal Cyclones**
Ian A Renfrew, Alan J Thorpe and Craig H Bishop
September 1997

75. **Potential Vorticity: A short history of its definitions and uses**
Alan J Thorpe and Hans Volkert
September 1997

76. **Superposing Semi-Geostrophic Potential Vorticity Anomalies**
H R Birkett and A J Thorpe
September 1997

77. **Short period forecasting of catchment-scale precipitation. Part 1: the role of Numerical Weather Prediction**
M A Pedder, M Haile and A J Thorpe
September 1997

78. **Verification of the Tracking Technique Used in an Experimental Cloud Motion Wind Inferring System**
Z Wang, K A Browning and G A Kelly
October 1997

**Met Office** Joint Centre for Mesoscale Meteorology Department of Meteorology
University of Reading PO Box 243 Reading RG6 6BB United Kingdom
Tel: +44 (0)118 931 8425 Fax: +44 (0)118 931 8791
www.metoffice.com